

Jet Cocoons and the Formation of Narrow Line Clouds in Seyfert Galaxies

W. Steffen¹, J.L. Gómez^{1,2}, R.J.R. Williams^{1,4}, A.C. Raga³, A. Pedlar⁵

¹*Department of Physics and Astronomy, University of Manchester, Schuster Laboratory, Oxford Road, Manchester M13 9PL, UK*

²*Instituto de Astrofísica de Andalucía, CSIC, Apdo. 3004, Granada 18080, Spain*

³*Instituto de Astronomía, UNAM, Apdo. Postal 70-264, 04510 Mexico, D.F., Mexico*

⁴*Dept. of Physics and Astronomy, The University, Leeds LS2 9JT, UK*

⁵*Nuffield Radio Astronomy Laboratories, University of Manchester, Jodrell Bank, Macclesfield, Cheshire SK11 9DL, UK*

ABSTRACT

We present non-adiabatic hydrodynamic simulations of a supersonic light jet propagating into a fully ionized medium of uniform density on a scale representative of the narrow line region (NLR) in Seyfert galaxies with associated radio jets. In this regime the cooling distance of the swept up gas in the bowshock of the jet is of the same order as the transverse extent of the jet bowshock, as opposed to the more extreme regimes found for more powerful adiabatic large scale jets or the slow galactic jets which have been simulated previously. We calculate the emissivity for the H α line and radio synchrotron emission. We find that the structure of the line emitting cold envelope of the jet cocoon is strongly dependent on the non-stationary dynamics of the jet head as it propagates through the ambient medium. We observe the formation of cloud-like high density regions which we associate with NLR clouds and filaments. We find that some of these clouds might be partially neutral and represent sites of jet induced star formation. The calculated H α flux and the spectral line width are consistent with NLR observations. The simulation of the radio-optical emission with radiative cooling confirms the basic result of the geometric bowshock model developed by Taylor et al. (1989) that the start of noticeable optical line emission can be significantly offset from the hotspot of the radio emission. However, the time-dependent nature of the jet dynamics implies significant differences from their geometric bowshock model.

Key words: galaxies: active - galaxies: jets - galaxies: kinematics and dynamics - galaxies: Seyfert - galaxies: individual: Mkn1066 - hydrodynamics: numerical

1 INTRODUCTION

The study of the Narrow Line Region (NLR) in Seyfert galaxies is contributing substantially to the understanding of the central engine of active galaxies. Of particular interest is the apparent close association between radio continuum and optical line emission in this region, which has a typical extent of 0.1-1 kpc. The link between optical and radio emission in the NLR manifests itself most prominently in a positional association between linear radio structures and optical line emission as well as in a correlation between line width and radio power (Wilson and Willis 1980, Whittle 1985). It is widely accepted that the radio emission is related to the outflow of relativistic plasma from the core of the galaxy. As is found in higher power radio galaxies and quasars, this outflow appears to be highly collimated into jets. The radio-optical association suggests that the interaction of the jets with the interstellar medium (ISM) strongly

influences the dynamics of the ionized gas in the NLR. It can be hoped that the study of this interaction will reveal important information on the physical conditions of the gas in the NLR and in the plasma jets.

The expansion of the cocoons of large scale extragalactic jets in radio galaxies has been examined analytically by Scheuer (1974) and Begelman and Cioffi (1989) and numerically by Cioffi and Blondin (1992). Blandford and Königl (1979) first suggested that the interaction of jets with BLR clouds could cause the radio emission and the associated kinematics of the BLR. The observation of symmetric double or triple radio sources associated with emission line gas in the NLR of a number of Seyfert galaxies (in particular in NGC 5929, Haniff, Wilson and Ward 1988, Su et al. 1996, and NGC 1068, Wilson and Ulvestad 1987, Gallimore et al. 1996) led to the development of more detailed models invoking the interaction of plasmons or jets with the local ISM. Pedlar et al. (1985) proposed an expanding plasmon

model for the NLR. They suggested that a high pressure relativistic plasma bubble expands and drives a shock wave sweeping up the surrounding ISM.

Whittle et al. (1986) found a spatial separation of $0.95 \pm 0.11''$ between the peaks of the [O III] 5007-Å components in high dispersion spectroscopic observations. This separation is significantly smaller than the measured distance between the radio components. Based on these observations, Pedlar et al. (1987) proposed a variant of the plasmon model similar to the radiative bowshock model suggested earlier by Wilson & Ulvestad (1987) for the radio structure observed in NGC 1068. This model explains the difference in the spatial separation between the peaks of the radio and the optical components. It invokes a supersonic motion of a jet or plasmon inducing a bowshock in the ambient medium. In the frame of the head of the bowshock, the shocked ISM gas then moves along its surface. All the basic properties of an expanding plasmon model are still applicable, but, in addition, the cooling time of the gas behind the bowshock allows the gas to flow a significant distance from the vertex before cooling to a temperature sufficiently low ($\sim 10^4$ K) that optical lines are emitted. Since the radio emission is expected to peak at the vertex, there will be a difference in the peak positions of the optical and the radio emission. This model was further developed by Taylor et al. (1989, 1992) and Ferruit et al. (1996).

Recent Hubble Space Telescope (e.g. Capetti et al. 1995a,b; Bower et al. 1994, 1995) and MERLIN observations (Pedlar et al. 1993; Kukula et al. 1996) revealed overwhelming new structure in the NLR of several Seyfert galaxies with radio jets. Discrete clouds and diffuse line emission are found to be closely aligned with highly structured and sometimes distorted radio jets. These observations clearly show that the idea of a radio jet interacting with the NLR can account for basic features of these jets. However, the phenomena are far more complicated than can be accounted for by the simple geometric bowshock model. The full non-stationary character of the interaction between a jet and its environment has to be taken into account to explain the newly observed features.

In this paper, we therefore apply high resolution axisymmetric hydrodynamic simulations to explore the time dependent interaction of Seyfert jets with the NLR. We demonstrate that the association between the radio and optical emission can be explained as a natural consequence of the expansion of a hot jet cocoon into the interstellar medium creating an envelope of dense cool gas and discrete emission line knots which can be associated with the narrow-line clouds themselves. We compare our model with observations of the NLR H α emission in MKN 1066, which has a similar linear extension (Bower et al. 1995).

In Section 2 we estimate the properties of our cocoon shock model analytically. The numerical procedure of the simulations is briefly described in Section 3. Section 4 contains the results and their discussion. We summarize our conclusions in Section 5.

2 ANALYTICAL ESTIMATES

We consider the dense optically emitting envelope of swept-up ISM gas around the cocoon of a supersonic jet propa-

gating into a uniform, ionized medium. The ionization is assumed to be due to photoionization from a UV source at the active nucleus of the galaxy. For a UV photon rate $S \sim 10^{52} \text{ s}^{-1}$ similar to the one in NGC 5929 (Bower et al. 1995) and an ambient density of 1 cm^{-3} the radius of the Strömgren sphere is 700 pc, which is well beyond the distances we consider in this paper. For an estimate of the initial conditions in a simulation which can be compared with typical observations, we assume that the envelope is a thin cylindrical shell of radius $r_c \sim 20 \text{ pc}$, length $l_c = 150 \text{ pc}$, H α luminosity $L_{\text{H}\alpha} = 10^{37} - 10^{39} \text{ erg s}^{-1}$, and a thickness $d_c \ll r_c$. Within our model the spectral line width in the NLR will be similar to twice the cocoon expansion speed, if observed from a direction perpendicular to the jet axis. We therefore have typical shock velocities of 100–200 km s^{-1} (e.g. MKN 1066, Bower et al. 1995). In the following, we estimate some characteristic quantities, such as the density n_0 of the ambient ISM, the density n_c and thickness d_c of the dense cool envelope, using this range of observed sizes and luminosities.

2.1 Non-magnetic case

We first assume that there is no magnetic field in the environment which could limit the compression at the shock, which is driven perpendicularly to the jet axis into the ISM by the overpressured cocoon. We further assume that the shock is isothermal, at the temperature $T_0 = 10^4 \text{ K}$ of the pre-shock gas. This assumption is justified by estimating the cooling distance δ behind a shock of speed $v_s = 150 \text{ km s}^{-1}$ in typical environmental gas with a hydrogen density of $n_0 = 1 \text{ cm}^{-3}$, using the adiabatic compression factor of 4. We then have (Taylor, Dyson and Axon 1992)

$$\delta = \frac{\bar{m} v_s k T_s^{(1-\alpha)}}{4 m_p n_0 \Lambda_0}, \quad (1)$$

where we use a power-law cooling function of the form

$$\Lambda(T_s) = \Lambda_0 T_s^\alpha \quad (2)$$

with $\Lambda_0 = 4.6 \cdot 10^{-18} \text{ erg s}^{-1} \text{ cm}^3$ and $\alpha = -0.76$ at $T > 1.5 \cdot 10^5 \text{ K}$. The temperature T_s immediately behind the shock is given by

$$T_s = \frac{3}{16} \frac{\bar{m}}{k} v_s^2, \quad (3)$$

where \bar{m} is the mean molecular weight and k is the Boltzmann constant (we assume $\bar{m} = 0.5 m_p$, m_p is the proton mass). The cooling distance perpendicular to the shock is then $\delta = 1.8 \cdot 10^{17} \text{ cm}$ or 0.06 pc with corresponding postshock temperature of $T_s = 2.5 \cdot 10^5 \text{ K}$. For $v_s = 100$ (200) km s^{-1} the cooling distance will be 2.2 (3.7) times smaller (larger) than for $v_s = 150 \text{ km s}^{-1}$. All these values are much smaller than the radius $r_c \sim 20 \text{ pc}$ of the cocoon, justifying the assumption of an isothermal shock for the estimates.

We now calculate the density n_c and thickness d_c of the compressed postshock layer of gas and the density of the environmental gas n_0 . We start with the compression ratio of the isothermal shock, which is

$$f = \frac{n_c}{n_0} = \frac{\bar{m} v_s^2}{k T_0} = 120 \frac{\bar{m}}{m_p} \left(\frac{T_0}{10^4 \text{ K}} \right)^{-1} \left(\frac{v_s}{100 \text{ km s}^{-1}} \right)^2 \quad (4)$$

In terms of the volumes of the cylindrical cocoon V_z and the cylindrical shell of swept up gas around the cocoon V_c we also have

$$f = \frac{V_z}{V_c} = \frac{\pi r_c^2 l_c}{2\pi r_c d_c l_c} = \frac{r_c}{2d_c}. \quad (5)$$

Combining equations (4) and (5) we find the thickness of the layer of swept up gas to be

$$\begin{aligned} d_c &= \frac{r_c kT_0}{2 \bar{m} v_s^2} \\ &= 0.083 \text{ pc} \frac{\bar{m}}{m_p} \left(\frac{r_c}{20 \text{ pc}} \right) \left(\frac{T_0}{10^4 \text{ K}} \right) \left(\frac{v_s}{100 \text{ km s}^{-1}} \right)^{-2} \end{aligned} \quad (6)$$

Assuming pure hydrogen gas of uniform density, the $\text{H}\alpha$ luminosity of this layer will be

$$\begin{aligned} L_{\text{H}\alpha} &= n_c^2 \epsilon V_c \\ &= 3.7 \times 10^{38} \text{ erg s}^{-1} \left(\frac{n_c}{100 \text{ cm}^{-3}} \right)^2 \left(\frac{V_c}{10^{59} \text{ cm}^3} \right) \end{aligned} \quad (7)$$

where $\epsilon = 3.8 \times 10^{-25} \text{ erg cm}^3 \text{ s}^{-1}$ is the $\text{H}\alpha$ emission coefficient at T_0 (see Section 3.4.1).

The total mass swept up from the environment into the shell is

$$M = n_c m_p V_c = 8300 M_\odot \left(\frac{n_c}{100 \text{ cm}^{-3}} \right) \left(\frac{V_c}{10^{59} \text{ cm}^3} \right) \quad (8)$$

We assume full ionization of the gas in the NLR. A column of swept up hydrogen gas of density n_c at a distance l_c from the ionizing photon source with a photon flux S will stay fully ionized up to a thickness

$$d_s = 1.1 \text{ pc} \left(\frac{n_c}{100 \text{ cm}^{-3}} \right)^{-2} \left(\frac{l_c}{100 \text{ pc}} \right)^{-2} \left(\frac{S}{10^{52} \text{ s}^{-1}} \right) \quad (9)$$

assuming that no photons are intercepted on their way to the cloud.

In Section 4 we compare these analytic estimates with the results from our simulation.

2.2 Magnetic case

We now consider the case where the undisturbed environment is threaded by a random magnetic field, assuming the components in the plane of the shock will be compressed with the field lines frozen into the gas. The effect of the magnetic field will be to limit the compression of the shocked gas when the magnetic pressure equals the thermal pressure. The compression factor f_m is then given by (e.g. Dopita and Sutherland 1995):

$$\begin{aligned} f_m &= \frac{n_{cm}}{n_{0m}} = \frac{(8\pi \bar{m})^{1/2} v_s}{B_{\parallel} n_{0m}^{-1/2}} \\ &= 64 \frac{\bar{m}}{m_p} \left(\frac{v_s}{100 \text{ km s}^{-1}} \right) \left(\frac{B_{\parallel} n_{0m}^{-1/2}}{\mu \text{G cm}^{-3/2}} \right) \end{aligned} \quad (10)$$

The thickness of the shocked gas layer is then

$$\begin{aligned} d_{cm} &= \frac{r_c B_{\parallel} n_{0m}^{-1/2}}{2v_c (8\pi \bar{m})^{1/2}} \\ &= 0.15 \text{ pc} \bar{m} m_p^{-3/2} \left(\frac{r_c}{20 \text{ pc}} \right) \left(\frac{v_s}{100 \text{ km s}^{-1}} \right)^{-1} \end{aligned}$$

$$\left(\frac{B_{\parallel} n_{0m}^{-1/2}}{\mu \text{G cm}^{-3/2}} \right). \quad (11)$$

Values of the magnetic parameter $(B_{\parallel} n_{0m}^{-1/2})/(\mu \text{G cm}^{-3/2})$ are of order 1, in the range 1-10 (Dopita & Sutherland, 1995).

Due to the additional magnetic pressure, the thickness of the cold envelope will be larger and the density lower than in the non-magnetic case. Since the optical line emission depends on the square of the density, the emission received from a strongly magnetized envelope will be considerably lower than that coming from a non-magnetic envelope.

3 NUMERICAL SIMULATION

3.1 Initial conditions

The determination of jet parameters like plasma speed and density is a classical and basically unsolved problem in extragalactic astrophysics. For the purpose of simulating the the expanding envelope, the exact values of the jet speed and density input parameters are not important. The expansion of the cocoon shock is principally determined by the cocoon pressure, and a given pressure can be obtained from a range of jet parameters. For practical purposes this range of parameters is also somewhat restricted by the available computing resources. We therefore performed a small series of test runs varying the particle density in the ISM around 1 cm^{-3} , jet velocities around 10^4 km s^{-1} (Bicknell et al. 1990) and Mach numbers around 10. A Mach number higher than 5 is required for a jet with a noticeable cocoon (Norman, Smarr and Winkler 1985). From these tests we chose a set of parameters which compares well with the observations of Seyfert galaxies given in Section 2 (in particular MKN 1066) and which illustrates best the qualitative features of the formation and structure of the dense cocoon envelope. A more detailed account on the influence of varying the parameters will be given in a forthcoming paper (Steffen et al., in preparation). The chosen parameters are:

$$\begin{aligned} n_0 &= 1.5 \text{ cm}^{-3} \\ T_0 &= 10^4 \text{ K} \\ n_j &= 0.18 \text{ cm}^{-3} \\ M_j &= 8.3 \\ v_j &= 6.8 \times 10^8 \text{ cm s}^{-1} \\ r_j &= 5.3 \times 10^{18} \text{ cm} \end{aligned}$$

This yields a jet mechanical luminosity of $L_j = 2 \times 10^{39} \text{ erg s}^{-1}$.

3.2 Scaling and similarity

In the absence of cooling, the jet will be evolve in a self-similar fashion

$$l_c = \mathcal{A} \left(\frac{L_j t^3}{\bar{m} n_0} \right)^{1/5} \quad (12)$$

with $\mathcal{A} \simeq 1$, once $l_c \gg (n_j/n_e)^{1/2} r_j = 2 \times 10^{18} \text{ cm}$ (Falle 1991).

Cooling will begin to have an effect when the advance speed of the outer shock at the base of the jet is roughly 100 km s^{-1} (Dyson 1984), that is roughly when $l_c = l_{\text{cool}} = 6 \times 10^{19} \text{ cm}$, if the aspect ratio of the jet is $\mathcal{R} = l_c/r_c = 5$. Thus, for our typical parameters, the jet will be self similar before cooling becomes important (neglecting the effects of turbulence in the jet).

Once cooling becomes non-negligible, self-similarity no longer holds but the evolution of jets with different parameters will be similar to each other, if times are scaled to the time at which the gas begins to cool, and distances are scaled to the length of the jet at this time. For the cooling law, equation (2), the lengths will scale as

$$l_{\text{cool}} \simeq 6 \times 10^{19} \text{ cm} \left(\frac{L_j}{2 \times 10^{39} \text{ erg s}^{-1}} \right)^{(3-2\alpha)/(9-4\alpha)} \cdot \left(\frac{n_0}{1.5 \text{ cm}^{-3}} \right)^{-(6-2\alpha)/(9-4\alpha)} \quad (13)$$

and the times as

$$t_{\text{cool}} \simeq 6 \times 10^{11} \text{ s} \left(\frac{L_j}{2 \times 10^{39} \text{ erg s}^{-1}} \right)^{(2-2\alpha)/(9-4\alpha)} \cdot \left(\frac{n_0}{1.5 \text{ cm}^{-3}} \right)^{-(7-2\alpha)/(9-4\alpha)} \quad (14)$$

If the jet power is doubled, the timescales will increase by 22 per cent and the lengthscales by 30 per cent, while if the ambient density is doubled the lengthscales will decrease by 35 percent and the timescales by nearly 40 per cent.

Once the cooling becomes rapid at the head of the jet, when $l_c \simeq \mathcal{R}^{3/2} l_{\text{cool}}$, the global evolution of the jet will enter a second self-similar regime with its evolution varying according to equation (12), only with a rather smaller constant of proportionality.

3.3 The hydrodynamic code

We used the adaptive grid hydrodynamic code described by Biro et al. (1995) in axisymmetric mode. It solves the equations of mass, momentum and energy conservation using a flux-vector-splitting scheme. The computation was carried out in a 5-level, binary adaptive grid. In our simulations we assume full ionization of the jet and ambient medium due to photoionization from the central UV source. We use the non-equilibrium cooling function described by Biro et al. (1995) with an additional term taking into account bremsstrahlung losses, L_b , given by

$$L_b = 2.29 \times 10^{-27} n_e n_p T_e^{\frac{1}{2}} \text{ erg s}^{-1} \text{ cm}^{-3} \quad (15)$$

where n_e and n_p are the electron and proton densities in particles per cm^3 , respectively, and T_e is the electron temperature in Kelvin (Cox & Tucker 1969). We do not allow the gas temperature to drop below 10^4 K , where we assume it is maintained by the thermostat effect of [O III] 5007-Å emission.

The computational domain was set to be 513×1025 computational cells and 5×1.25 times 10^{20} cm . The grid cells are smaller in radial direction than in axial direction for better resolution of the small distance scales of the radially expanding envelope. The initial jet radius was covered by 27 cells in the axisymmetric simulation. The cooling distance

δ was marginally resolved for $v_s = 150 \text{ km s}^{-1}$. The thickness d_c of the cold envelope of swept up gas was near the resolution limit and was smeared out artificially over 2-3 cells at shock speeds higher than 150 km s^{-1} . This artificially limits the compression with effects similar to those expected if magnetic fields in the ISM were present (with a magnetic parameter of the order of 5, although magnetic fields were not taken into account explicitly). However, increasing the resolution further would lead to prohibitively large computing times for these initial studies. Quantitative results will therefore be only order of magnitude estimates, but the qualitative results, as discussed in this paper, will not be significantly altered. The boundary conditions are reflective on the axis and on the left side of the computational domain (except for the inflow condition where the jet is injected, see Fig. 1). The top and right boundaries have outflow conditions.

3.4 Emission maps

3.4.1 Optical emission

We calculate the H α emissivity ϵ using radiative recombination (Case B) following Aller (1984). In the temperature regime of our simulations ($T > 10^4 \text{ K}$) only recombination contributes considerably to the emissivity. We assume full ionization of the hydrogen, which would mainly be due to photoionization from the UV source at the centre of the galaxy and, to some extent, from shock ionization in the bowshock region.

$$\epsilon = 4.16 \times 10^{-25} \text{ erg cm}^3 \text{ s}^{-1} (T_4^{0.983} 10^{0.0424/T_4})^{-1} \quad (16)$$

where T_4 is the temperature in units of 10^4 K .

3.4.2 Radio emission

Only relativistic electrons (and perhaps positrons) contribute significantly to the radio emission of jets. Since it is still unclear how these high energy electrons are generated (most probably through re-acceleration in shocks), we assume that this population of fast electrons shares the same hydrodynamics as the non-relativistic fluid of electrons and protons. A more detailed description would require the consideration of two jet populations to account for the non-relativistic gas (electrons and protons) with ratio of specific heats of 5/3, and the ultrarelativistic electrons with ratio of 4/3. Duncan, Hughes, Opperman (1996) have performed preliminary simulations of highly relativistic jets using a variable adiabatic index and found that the rest frame variables vary smoother along the jet axis, with smaller amplitude maxima at the bowshock, and in the vicinity of the contact surface. We ignore these effects in the present simulations.

In order to calculate the synchrotron emission from the jet whose hydrodynamics is modeled as above, we need to establish how the internal energy is distributed among the relativistic electrons. Observations suggest that this distribution follows the usual power law $N(E) dE = N_0 E^{-p} dE$, with spectral index p , and energies above a minimum value E_{min} . Assuming that the relativistic electron energy density \mathcal{U} , and number density \mathcal{N} are proportional to their corresponding thermal quantities calculated by the hydrodynam-

ical code as a function of position in the jet, the previous power law is determined by the equations (Gómez et al. 1995)

$$N_o = [\mathcal{U} (p-2)]^{p-1} [\mathcal{N} (p-1)]^{p-2} \quad (17)$$

and

$$E_{\min} = \frac{\mathcal{U}}{\mathcal{N}} \frac{p-2}{p-1}, \quad (18)$$

The synchrotron emission is also determined by the magnetic field, and since we are neglecting its influence on the fluid dynamics, we assume that the magnetic energy density remains a fixed fraction of the particle energy density, which leads to a field of magnitude proportional to $\mathcal{U}^{1/2}$. We refer the reader to Gómez et al. (1993, 1995) for a detailed discussion of the radio emission calculations.

4 RESULTS AND DISCUSSION

4.1 Structure

We show the results of our simulation at a time when the jet has reached a distance of approximately 150 pc from the injection point. This is 127 000 years after the jet switched on.

Fig. 1 shows the density (top) and the pressure (bottom) distribution on a logarithmic scale. We can identify several characteristic features which are marked in the schematic view shown in Fig. 2. The jet itself shows several recollimation shocks on the axis, best seen in the pressure image. At the tip of the jet, the termination shock generates high pressure and high temperature jet plasma. This plasma flows back into the hot jet cocoon, which surrounds the high speed jet. The jet cocoon is surrounded by a thick layer of hot gas from the interstellar medium which has passed through the bowshock. Near the head of the jet we find a thin layer of hot shocked gas from the ISM which further back turns into an even thinner, but cold and very dense envelope of the jet cocoon. This envelope is what distinguishes the NLR jet from adiabatic high power extragalactic jets. The fact that this envelope starts at a significant distance from the front of the bowshock distinguishes NLR jets from the regime of strongly cooling galactic jets (e.g. Blondin, Fryxell and Königl 1990).

We find that the radius of the cold envelope in the simulation is approximately 7.8×10^{19} cm and the expansion speed of the cocoon is somewhat above 100 km s^{-1} . The peak density in the envelope varies from values between 30 to 40 cm^{-3} over most of its extent, up to 100 cm^{-3} in the dense clouds. This corresponds to compression factor of 30 and 70, respectively. This is factors of 2 too low compared to Eq. (4), which is probably due to numerical smearing. This effect mimics a magnetic parameter of the order of 5 (see Eq. 11), which corresponds to a ambient magnetic field near $5\mu\text{G}$. The integrated $\text{H}\alpha$ luminosity at this timestep is $5.8 \times 10^{37} \text{ erg s}^{-1}$ and the envelope has a thickness of $d_c \sim 1 - 2 \times 10^{18}$ cm and volume of $V_c \sim 2 \times 10^{59} \text{ cm}^3$. These values are in good agreement with our analytical estimates and the results from optical observations of Seyfert galaxies with associated NLR radio jets.

We find that the non-stationary dynamics of jet propagation through interstellar medium have a strong influence

on the structure of the cold shell. The quasi-periodic recollimations of the jet cause the advance speed of the jet head to oscillate, thereby accumulating jet material in a restricted nose region for some period of time. It is then released into the cocoon almost explosively, when the jet expands and slows down again. This imposes a characteristic arc structure onto the bowshock and the cold shell of swept up gas. These arcs cool almost as a unity once catastrophic cooling sets in. This can be seen in Fig.3, where the density is shown at three different times with the same separation between them. While the head of the jet has advanced considerably between the first and second panel, the point where the cold dense envelope starts has not advanced appreciably. However, later, after the same timestep, the full arc has cooled. Therefore, a cooling distance for the bowshock measured from the head of the jet, as discussed by Taylor et al. (1989, 1992), can at best be only an average property.

At the positions where neighbouring arcs meet, the two shock waves cross at an angle near 90° . This interaction will produce a Mach shock at the vertex with an effective speed of $\sqrt{2}$ times the speeds of the incident shocks (supposing that they are the same). Correspondingly, the compression and the emissivity of the gas increase by factors of ~ 2 and ~ 4 , respectively. As a result of the radiative nature of the crossing shocks they merge to form short high density filaments and clouds, marked as ‘‘high density spots’’ and ‘‘intruding dense filaments’’ in Fig. 2. In the simulation the spots have peak densities between 80 and 100 cm^{-3} , consistent with the previously estimated additional compression by factors around 2. We suggest that these spots could be identified with the brightest discrete clouds in the NLR of some Seyfert galaxies. Note that the spacing between these spots is directly related to the time dependent quasi-periodic recollimation of the jet and therefore contains information about the history of the interaction between the jet and its environment. Several Seyfert galaxies show a knotty NLR structure and the distances between the strongest emission line clouds is indeed similar but rather smaller than the distances between the radio knots (e.g. MKN 3, Capetti et al. 1995a; MKN 6, Capetti et al. 1995b; NGC 4151, Boksenberg et al. 1995).

At some distance from the jet head the arc structure in the envelope is lost and it becomes roughly cylindrical justifying the approximations of Section 2 (Fig.1). However, the high density clouds and filaments created at the intersection points of these arcs are retained. When the envelope fragments (as can be expected in a full three dimensional simulation) these regions will be seen as discrete NLR clouds and filaments. Since the creation of these arcs and clouds is related to the recollimations of the jet, we have found a direct relation between the optical structure of the NLR and the internal non-stationary shock structure of the jet.

The expansion of the overpressured jet cocoon into the undisturbed interstellar medium is similar to a supernova explosion. Some theoretical aspects can therefore be treated in an analogous fashion. This applies in particular to the stability of the shock and the postshock layer of swept up gas. The stability of radiative shock wave has been considered by a number authors with varying emphasis (e.g. Vishniac 1983, Bertschinger 1986). The radiative shock instabilities discussed by Bertschinger (1986) are present in our simulations and produce the pressure variations near the cold en-

velope. These are likely to be disruptive and thus contribute to the formation of NLR clouds and filaments. From the results presented by Jun, Norman and Stone (1995) it can be expected that the shock region in our simulation is also Rayleigh-Taylor (R-T) unstable, with fastest growth of features on the scale of the thickness of the cold layer of swept up gas. The onset of these instabilities can be observed as pressure variations and small ripples in some sections of the cold envelope (Fig.1). As these instabilities grow, they might contribute to the fragmentation process of the envelope and form further NLR clouds, in addition to the high density clouds produce at the intersection of the arcs discussed in the previous section. However, magnetic fields have a stabilizing effect and therefore different combinations of ambient magnetic parameters and jet powers might lead to two categories of evolved cocoon envelopes: R-T stable narrow line regions with fewer small clouds and R-T unstable ones with a high number of small NLR clouds with separations of a few times the thickness of the cold layer (i.e. ~ 1 pc). More detailed investigations of this process will have to be carried out to quantify this prediction over a range of parameters in order to compare it with recent and future high resolution observations of the NLR in Seyfert galaxies.

The Strömngren column given by Eq.(9) is similar to the thickness of the cocoon envelope and the size of the clouds. It may well be that the highest density clouds can develop neutral cloud cores. As a result, NLR clouds could be sites of jet induced star formation (Van Breugel and Dey 1993, Tresch-Fienberg et al. 1987).

4.2 Emission

In Fig.4 the $H\alpha$ emissivity distribution is displayed on a logarithmic along with the radio emission superimposed as contours in the lower panel. As expected, most of the optical line emission comes from the thin envelope of cold postshock material. The $H\alpha$ luminosity obtained from this axisymmetric simulation is $5.8 \times 10^{37} \text{erg s}^{-1}$. This is well within our expectations considering the simplicity of our analytical estimates. The length of the NLR jet in MKN 1066 is similar to that in our simulation, although the transverse extent could be 2-3 times smaller. From observations by Bower et al. (1995) we determined the $H\alpha$ flux coming from the area covered by the NE jet in MKN 1066 to be $3.3 \times 10^{37} \text{erg s}^{-1}$, which is in excellent agreement with our simulation, taking into account the the simplifications of the model and the smaller radius of the cocoon in MKN 1066.

From our model it can be expected that higher power radio jets yield faster cocoon shocks, producing broader emission lines. This will result in a correlation between line width and radio power, which is consistent with the observed correlation between these quantities (Wilson and Willis 1980, Whittle 1985). Our initial study does, however, not allow a more quantitative conclusion about the correlation. An extensive survey of the parameter space and other factors which influence the line width, like galaxy rotation, is needed for a detailed theoretical study of this correlation in terms of our model.

The calculated line spectrum is shown in Fig.5 for three different viewing angles. In the spectrum, emission from the background has not been included in order to focus on the expanding envelope. Inclusion of the background would

produce a narrow peak at zero velocity. Within the volume of this simulation the background emission amounts to $4.8 \times 10^{36} \text{erg s}^{-1}$, an order of magnitude less than contained in the envelope. The strength of this central peak, compared to the broader contribution from the envelope, is a measure of the ratio of disturbed and undisturbed gas. Because of the cylindrical shape of the expanding envelope and the small velocity of the gas along the shell, the line shape of the envelope is double peaked for viewing angles far from the axis but becomes almost rectangular if the line of sight is near the jet axis. The line width of the expanding cylindrical shell is, of course, not only a function of the expansion speed (which is approximately the same as the shock speed), but depends also on the angle between the symmetry axis and the line of sight. This is in apparent disagreement with results from Whittle (1985), which suggest that there is no strong correlation between the orientation of the galaxy and the NLR line width, assuming that the jet follows the rotation axis of the galaxy. However, observations of radiation cones (e.g. Wilson and Tsvetanov 1994), which at least can be expected to have a closer link to the radio jets, and point symmetric bending of jets in Seyferts (presumably as a result of the interaction with the rotating environment, Wilson and Ulvestad 1982, Steffen et al. 1996) suggest that the jets often are not aligned with the rotational axis of the galaxies. This would strongly weaken any correlation between line width and galaxy rotation.

The contours in Fig.4 show the radio emission at 10 GHz as calculated from our model described in Section 3.4.2. A spectral index in the power law energy distribution of the electrons of 2.4, and magnetic field strength at the jet inlet of $100 \mu\text{G}$ have been used. A total flux for the jet of 4 mJy is obtained. As expected, most of the radio emission comes from the hotspot region near the head of the jet, with some low brightness emission from the recollimation shocks. There are a number of Seyfert jets in which the head of the jet is dominant at radio wavelength. However, in most cases there are a number of strong radio knots along the jet. More so in the case of NGC 1066, which has rather continuous emission along the jet (at the resolution of the VLA) and no hot spot near the head. This highlights the problem of the nature of the knots seen along radio jets in general. Internal shocks can produce this kind of knots. In our simulations we find two different types of internal shocks: the recollimation shocks and the shocks produced by the interaction with the turbulent cocoon near the head of the jet. From our simulations and our model for the synchrotron emission we find that these are not strong enough to explain the radio emission knots seen in most of the Seyfert jets. One possible solution are time variations of the ejection parameters at the base of the jet. Gómez et al (1996), Hughes, Duncan, and Mioduszewski (1996) and Komissarov and Falle (1996) have shown that variations of the ejection velocity can produce strong internal working surfaces which visible as strong radio knots in the jet. Such variations in the jet properties possibly have some influence on the structure of the cold cocoon envelope and thus on the NLR. In a forthcoming paper we will investigate the effects of variable jet properties on the NLR in more detail (Steffen et al, in preparation).

5 CONCLUSIONS

Using hydrodynamic simulations with radiative cooling we confirm the basic structure of the interaction between a jet and the NLR in Seyfert galaxies as obtained in a geometric model by Taylor et al. (1989). However, we find new features of the interaction, like the formation of NLR clouds and a larger extent of the cold cocoon envelope. Due to the time-dependent propagation speed of the jet into the ISM, the cooling distance of the bowshock material as measured from the head the jet varies episodically with time. Our simulations show that there might be a link between the time-dependent internal collimation structure of the radio jets and the narrow line clouds. We expect that the distances between particularly bright knots along the symmetry axis are similar to the separation between the radio knots behind the main hotspot (assuming that the latter are due to internal recollimation shocks). Estimates of the Strömgren column show that the dense clouds produced in this simulation could be partially neutral. They might represent cores for jet induced star formation in the NLR of Seyfert galaxies.

6 ACKNOWLEDGEMENTS

We thank F. Kahn, J.E. Dyson, J. Meaburn, and D.J. Axon for useful discussions. We also thank the referee S.A.E.G. Falle for useful suggestions. WS, JLG and RJRW acknowledge the receipt of a PPARC associateship. JLG also gratefully acknowledges a “Contrato de Reincorporación” by the Spanish Ministry of Education.

REFERENCES

Aller L., 1984, *Physics of Thermal Gaseous Nebulae*. Reidel, Dordrecht, 76
 Begelman M.C., Cioffi D.F., 1989, *ApJL*, 345, L21
 Bertschinger E., 1986, *ApJ*, 304, 154
 Bicknell G.V., de Ruiter H.R., Fanti R., Morganti R., Parma P., 1990, *ApJ*, 354, 98
 Biro S., Raga A.C., Cantó, 1995, *MNRAS*, 275, 557
 Blandford R.D., Königl A., 1979, *ApJ*, 232, 34
 Blondin J.M., Fryxell B.A., Königl A., 1990, *ApJ*, 360, 370
 Boksenberg A., Catchpole R.M., Macchetto F., et al., 1995, *ApJ*, 440, 151
 Bower G., Wilson A., Mulchaey J., 1994, *AJ*, 107, 1686
 Bower G., Wilson A., Morse J.A., Gelderman R., Whittle M., Mulchaey J., 1995, *ApJ*, 454, 106
 Capetti A., Macchetto F., Axon D.J., Sparks W.B., Boksenberg A., 1995a, *ApJ*, 448, 600
 Capetti A., Axon D.J., Kukula M., Macchetto F., Pedlar A., Sparks W.B., Boksenberg A., 1995b, *ApJL*, 454, L85
 Cioffi D.F., Blondin J.M., 1992, *ApJ*, 392, 458
 Cox D.P., Tucker W.H., 1969, *ApJ* 157, 1157
 Dopita M., Sutherland R.S., 1995, *ApJ*, 455, 468
 Duncan C., Hughes P., Opperman J., 1996, in *Energy Transport in Radio Galaxies and Quasars*, ASP Conference Series, Vol. 100, eds. P.E. Hardee, A.H. Bridle, and J.A. Zensus, p. 143
 Dyson J.E., 1984, *Ap&SS*, 106, 181
 Falle S.A.E.G., 1991, *MNRAS*, 250, 581
 Ferruit P., Binette L., Sutherland R.S., Pécontal E., A&A, submitted
 Gallimore J.F., Baum S.A., O’Dea C.P., Pedlar A., 1996, *ApJ*, 458, 136
 Gómez J. L., Alberdi, A., Marcaide J. M, 1993, *A&A*, 274, 55

Gómez J. L., Martí J.M^a, Marscher A.P., Ibañez J.M^a, Marcaide J.M., 1996, in *Energy Transport in Radio Galaxies and Quasars*, ASP Conference Series, Vol. 100, eds. P.E. Hardee, A.H. Bridle, and J.A. Zensus, p. 159
 Gómez J. L., Martí J. M^a, Marscher A. P., Ibañez J.M^a, Marcaide J. M, 1995, *ApJL*, 449, L19
 Haniff C.A., Wilson A.S., Ward M.J., 1988, *ApJ*, 334, 104
 Hughes P., Duncan C., Mioduszewski A., 1996, in *Energy Transport in Radio Galaxies and Quasars*, ASP Conference Series, Vol. 100, eds. P.E. Hardee, A.H. Bridle, and J.A. Zensus, p. 137
 Jun B.-I., Norman M.L., Stone J.M., 1995, *ApJ*, 453, 332
 Kommissarov S.S., Falle S.A.E.G., 1996, in *Energy Transport in Radio Galaxies and Quasars*, ASP Conference Series, Vol. 100, eds. P.E. Hardee, A.H. Bridle, and J.A. Zensus, p. 165
 Kukula M.J., Holloway A.J., Pedlar A., Meaburn J., López J.A., Axon D.J., Schilizzi R.T., Baum S.A., 1996, *MNRAS*, 280, 1283
 Norman M.L., Smarr L., Winkler K.-H. A., 1985, in *Numerical Astrophysics*, Centrella J., LeBlanc J., Bowers R., Wilson J.R., eds, Jones and Bartlett Publisher, p88
 Pedlar A., Dyson J.E., Unger S.W., 1985, *MNRAS*, 214, 463
 Pedlar A., Unger S.W., Dyson J.E., Axon D.J., 1987, *Star Formation in Galaxies*, NASA Conference Publ. 2466, p711
 Pedlar A., Kukula M.J., Longley D.P.T., Muxlow T.W.B., Axon D.J., Baum S., O’Dea C.O., Unger S.W., 1993, *MNRAS*, 263, 471
 Scheuer P.A.G., 1974, *MNRAS*, 166, 513
 Steffen W., Holloway A.J., Pedlar A., 1996, *MNRAS*, 282, 130
 Su B. M., Muxlow T. W. B., Pedlar A., Holloway A. J., Steffen W., Kukula M. J., Mutel R. L., 1996, *MNRAS*, 279, 1111
 Taylor D., Dyson J.E., Axon D.J., Pedlar A., 1989, *MNRAS*, 240, 487
 Taylor D., Dyson J.E., Axon D.J., 1992, *MNRAS*, 255, 351
 Tresch-Fienberg R., Fazio G.G., Gezari D.Y., et al., 1987, *ApJ*, 312, 542
 Van Breugel W.J.M., Dey A., 1993, *ApJ*, 414, 563
 Vishniac E.T., 1983, *ApJ*, 274, 152
 Whittle M., 1985, *MNRAS*, 216, 817
 Whittle M., Haniff C.A., Ward M.J., Meurs E.J.A., Pedlar A., Unger S.W., Axon D.J., Harrison B.A., 1986, *MNRAS*, 222, 189
 Wilson A., Tsvetanov Z.I., 1994, *AJ*, 107, 1227
 Wilson A., Ulvestad J.S., 1982, *ApJ*, 263, 576
 Wilson A., Ulvestad J.S., 1987, *ApJ*, 319, 105
 Wilson A., Willis A.G., 1980, *ApJ*, 240, 429

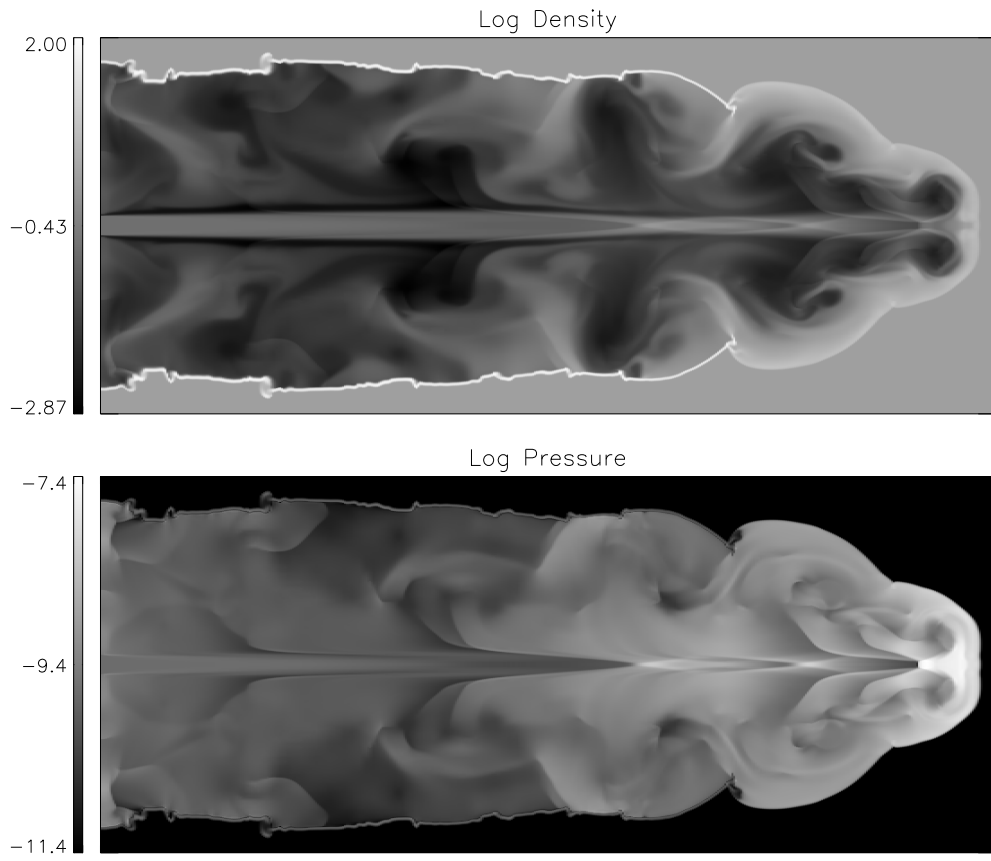


Figure 1. Density (top panel) and pressure (bottom panel) distribution on a logarithmic scale after 127 kyr. Note the high-density cocoon envelope after the swept up ISM-material has cooled to the equilibrium temperature of 10^4 K. The recollimation shocks and the very high pressure near the jet shock can clearly be seen in the pressure image.

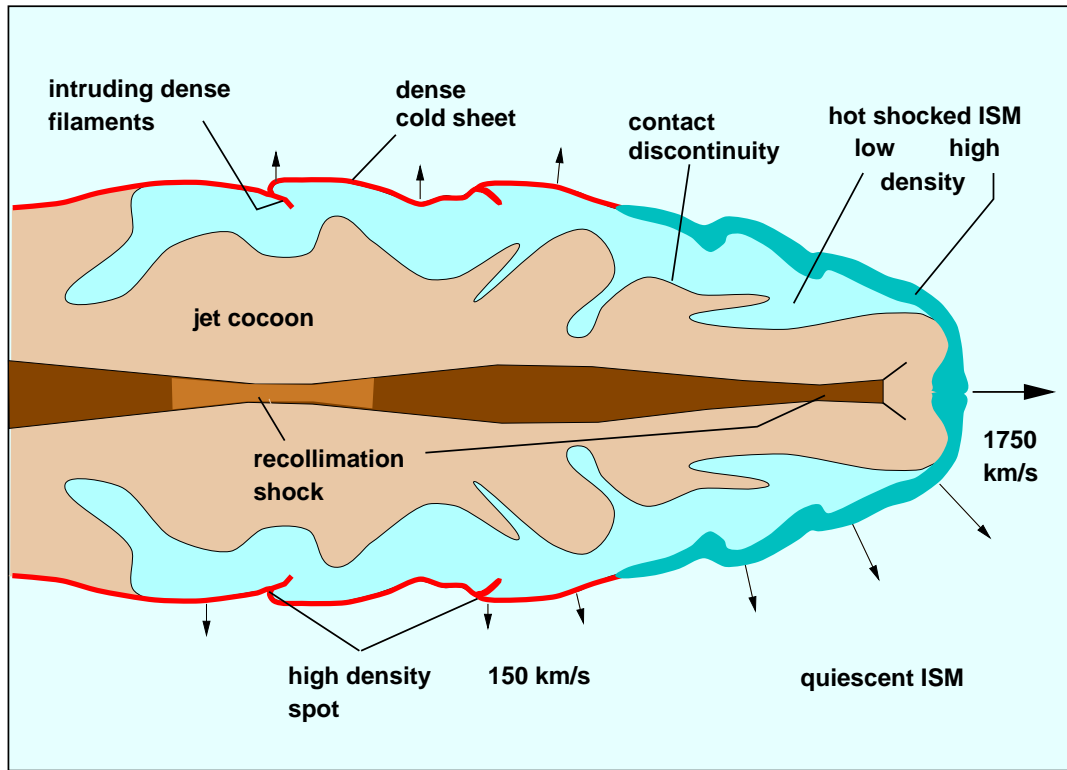


Figure 2. A schematic summary of the features seen in our hydrodynamic simulations. It includes the jet with recollimation shocks, the jet-shock, the cocoon of jet plasma, the hot bowshock and the cold layer shocked ISM.

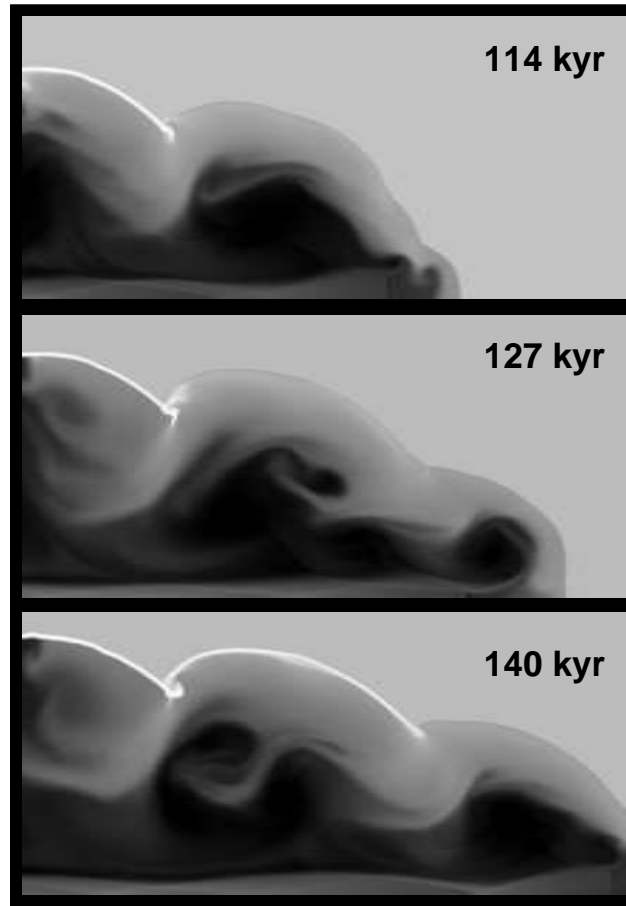


Figure 3. The bowshock structure (using the $H\alpha$ emissivity) is shown at three different times with the same separation between them. While the head of the jet has advanced considerably between the first and second panel, the point where the cold envelope starts has not advanced appreciably. After a further timestep, a full arc has collapsed and cooled and has become very bright.

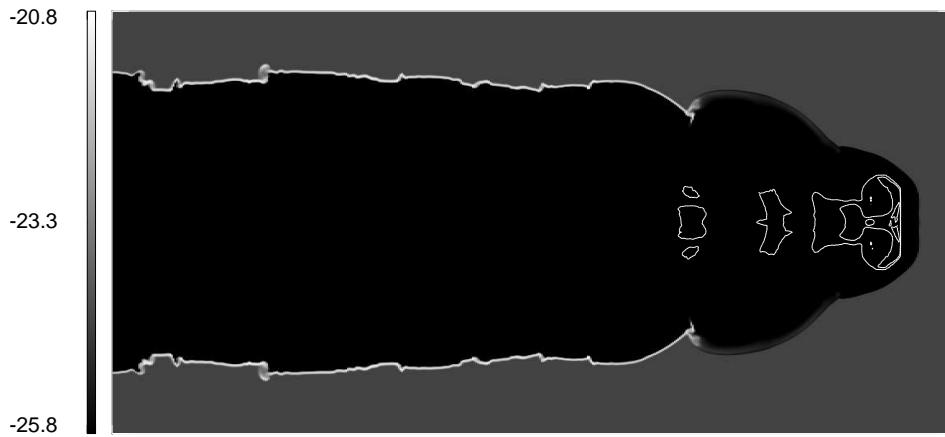


Figure 4. The $H\alpha$ emissivity map is shown on a logarithmic scale along with the calculated radio emission at 10 GHz superimposed as contours (radio contours are drawn for 0.6, 5 and 50 percent of peak brightness). Most of the optical emission comes from the thin envelope of swept up and cooled ISM gas. Particularly high emissivity regions are found where the bowshock ‘arcs’ intersected when still near the head of the jet. The radio emission is concentrated near the head of the jet, where temperature and pressure of the jet plasma is highest after passing through the jet shock.

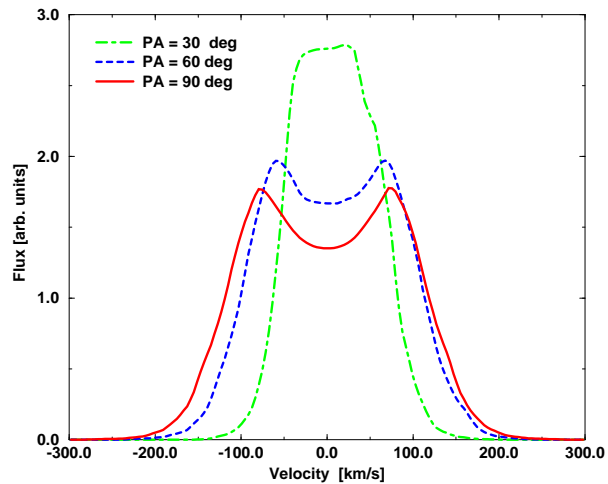


Figure 5. The spectral line shape of the $H\alpha$ emissivity distribution as seen from different angles between the line of sight and the jet axis is shown. For large angles the line is double peaked, but for angles near the jet axis the shape is rather rectangular.